J. Fluid Mech. (2020), *vol*. 900, A4. © The Author(s), 2020.
Published by Cambridge University Press
doi:10.1017/jfm.2020.456

Swimming with swirl in a viscoelastic fluid

Jeremy P. Binagia[1],†, Ardella Phoa[2], Kostas D. Housiadas[3] and Eric S. G. Shaqfeh[1]

[1]Department of Chemical Engineering, Stanford University, Stanford, CA 94305, USA

[2]Department of Bioengineering, Santa Clara University, Santa Clara, CA 95053, USA

[3]Department of Mathematics, University of the Aegean, Karlovassi, Samos 83200, Greece

(Received 9 February 2020; revised 9 February 2020; accepted 2 June 2020)

Microorganisms are commonly found swimming in complex biological fluids such as mucus and these fluids respond elastically to deformation. These viscoelastic fluids have been previously shown to affect the swimming kinematics of these microorganisms in non-trivial ways depending on the rheology of the fluid, the particular swimming gait and the structural properties of the immersed body. In this report we put forth a previously unmentioned mechanism by which swimming organisms can experience a speed increase in a viscoelastic fluid. Using numerical simulations and asymptotic theory we find that significant swirling flow around a microscopic swimmer couples with the elasticity of the fluid to generate a marked increase in the swimming speed. We show that the speed enhancement is related to the introduction of mixed flow behind the swimmer and the presence of hoop stresses along its body. Furthermore, this effect persists when varying the fluid rheology and when considering different swimming gaits. This, combined with the generality of the phenomenon (i.e. the coupling of vortical flow with fluid elasticity near a microscopic swimmer), leads us to believe that this method of speed enhancement could be present for a wide range of microorganisms moving through complex fluids.

Key words: micro-organism dynamics, viscoelasticity

1. Introduction

Recently, scientists have taken a keen interest in the motion of microorganisms swimming in complex fluids (Spagnolie 2015; Patteson, Gopinath & Arratia 2016). Examples of microscopic 'swimmers' moving through complicated biofluids abound: spermatozoa swims through the cervical mucus of the reproductive tract (Fauci & Dillon 2006; Suarez & Pacey 2006; Katz, Mills & Pritchett 2008), the bacteria *Escherichia coli* resides in the mucus of the intestine (Sillankorva, Oliveira & Azeredo 2012) and *Borrelia burgdorferi* (the organism responsible for causing Lyme disease) must traverse the extracellular matrix of mammalian skin (Harman *et al.* 2012). In each of these cases, the fluid in which the microorganism is immersed exhibits non-Newtonian behaviour due to the presence of large biological molecules creating a rich underlying microstructure (Spagnolie 2015). Understanding motility in these environments is not only interesting from a scientific perspective, but may also aid researchers in a variety of engineering applications, including preventing the spread of disease by disrupting biofilm

† Email address for correspondence: jbinagia@stanford.edu

formation (Costerton, Stewart & Greenberg 1999). A fundamental understanding of how microorganisms propel in complex fluids also enables the development of more advanced synthetic swimmers, which have been designed for targeted drug delivery (Patra *et al.* 2013; Gao & Wang 2014), minimally invasive surgery (Yan *et al.* 2017) and various other biomedical applications (Li *et al.* 2017).

It is now known that elasticity can impact the ability of an organism to swim, but this varies greatly depending on the kinematics of the gait (Godínez *et al.* 2015; Elfring & Goyal 2016), the structural properties of the immersed body and the rheology of the surrounding fluid (Dasgupta *et al.* 2013). In many cases, it has been observed that fluid elasticity can lead to a decrease in the swimming speed (Fu, Powers & Wolgemuth 2007; Lauga 2007; Fu, Wolgemuth & Powers 2009; Shen & Arratia 2011; Zhu *et al.* 2011; Zhu, Lauga & Brandt 2012; Binagia, Guido & Shaqfeh 2019). One may then ask under what conditions can elasticity actually enhance the speed of a swimming microorganism? Several mechanisms for viscoelastic speed enhancement have been put forth, beginning with Teran, Fauci & Shelley (2010), who showed that large-amplitude undulatory motion could lead to a speed increase. Shortly thereafter, Liu, Powers & Breuer (2011) and Spagnolie, Liu & Powers (2013) found that large-amplitude motion was also required to observe a speed enhancement for the case of helical motion. Thomases *et al.* and Riley *et al.* later demonstrated the importance of the elasticity of the immersed body, finding that microorganisms with sufficiently flexibility would swim faster in viscoelastic fluids (Riley & Lauga 2014; Thomases & Guy 2014, 2017). Lastly, phase separation resulting from the depletion of polymer molecules near bacterial flagellum creates an apparent slip that allows microorganisms to swim faster in shear-thinning fluids (Martinez *et al.* 2014; Man & Lauga 2015; Zöttl & Yeomans 2019).

In this report we propose an alternative mechanism for the speed enhancement of swimming microorganisms that originates from the coupling of fluid elasticity and local swirling flow. Indeed, previous studies have demonstrated that rotational motion can engender net translational motion in a viscoelastic fluid via hoop stresses that are created by the stretching of polymer molecules around the immersed body (Pak *et al.* 2012; Rogowski *et al.* 2018; Puente-Velázquez *et al.* 2019). To date, however, no one has explicitly considered how this rotational–translational coupling may affect the propulsion of self-propelled swimming microorganisms. Certainly, it is not immediately clear what the effect will be; while the aforementioned studies consider a synthetic swimmer driven to rotate by an applied torque (created for example by a rotating magnetic field), swimming microorganisms are wholly self-propelled, capable of swimming in the absence of any external forces/torques. In studying this phenomenon, we are particularly motivated by recent experimental work studying the motion of *E. coli* in a viscoelastic fluid (Patteson *et al.* 2015). There, it was hypothesized that the increase in speed as a function of polymer concentration that was observed (Patteson *et al.* 2016) might be a result of normal stress differences that could decrease cell 'wobbling' and create straighter and longer swimming trajectories. In this study we use a combination of numerical simulations and asymptotic theory to show that even a microswimmer constrained to swim in a straight line will experience a speed enhancement in a viscoelastic fluid so long as there is sufficient azimuthal swirl in its gait.

2. Mathematical model

2.1. *The squirmer model*

We first introduce the squirmer model (Lighthill 1952; Blake 1971), which is a spherical microscopic swimmer with a prescribed gait (given as a slip velocity at its surface).

This model has been widely used in the area of biological fluid mechanics to better understand the hydrodynamics of swimming microorganisms (Pedley 2016). It has especially been used to examine the effect that complex fluid rheology has on the swimming dynamics (Lauga 2009; Zhu *et al.* 2011; Zhu, Lauga & Brandt 2012; Li, Karimi & Ardekani 2014; Datt *et al.* 2015, 2017; De Corato *et al.* 2015; Datt & Elfring 2019; Pietrzyk *et al.* 2019). The general slip velocity for a steady axisymmetric squirmer exhibiting purely tangential deformations is given by Pak & Lauga as (Pak & Lauga 2014)

$$\boldsymbol{u}^s(\theta,\phi) = \sin(\theta)\left\{\sum_{n=1}^{\infty}\frac{2P_n'}{(n+1)n}B_n\boldsymbol{e}_\theta + \sum_{n=1}^{\infty}\frac{P_n'}{a^{n+1}}C_n\boldsymbol{e}_\phi\right\}, \tag{2.1}$$

where a is the squirmer's radius, θ is the polar angle ($0 \le \theta \le \pi$) and ϕ is the azimuthal angle ($0 \le \phi < 2\pi$); $P_n'(\mu)$ is the first derivative of the Legendre polynomial of degree n, where $\mu = \cos(\theta)$. The polar and azimuthal squirming modes are given by B_n and C_n, and $\boldsymbol{e}_\theta$ and $\boldsymbol{e}_\phi$ are the unit vectors in the polar and azimuthal directions, respectively.

Typically, authors only consider the first two polar squirming modes, those related to the coefficients B_1 and B_2 in (2.1). This is usually done because in a Newtonian fluid the swimming speed is determined solely by the value of B_1, i.e. $U_N = \frac{2}{3}B_1$ (Lighthill 1952; Blake 1971), while B_2 is the only coefficient appearing in the particle stresslet (Ishikawa, Simmonds & Pedley 2006). Furthermore, these are the only two modes necessary to differentiate between pushers, i.e. swimmers who generate thrust from behind their body (e.g. *E. coli*) and pullers, swimmers who generate thrust from the front of their body (e.g. *Chlamydomonas reinhardtii*). Only recently have authors started to consider the effect of higher-order polar squirming modes (Datt *et al.* 2015; De Corato & D'Avino 2017; Pietrzyk *et al.* 2019) or the azimuthal squirming modes (Ghose & Adhikari 2014; Pak & Lauga 2014; Felderhof & Jones 2016; Pedley 2016; Pedley, Brumley & Goldstein 2016). To date, however, no one has considered how the presence of the azimuthal modes of the squirmer model impacts swimming kinematics in a complex fluid.

2.2. *Governing equations*

We proceed by considering the flow generated by the swimming microorganism, which must obey conservation of momentum and the continuity equation. In dimensionless form these equations are given by

$$Re\left(\frac{\partial \boldsymbol{u}}{\partial t} + \boldsymbol{u}\cdot\nabla\boldsymbol{u}\right) = \nabla\cdot\boldsymbol{\sigma}, \quad \nabla\cdot\boldsymbol{u} = 0, \tag{2.2a,b}$$

where $\boldsymbol{u}$ is the fluid velocity, p is pressure and $\boldsymbol{\sigma}$ is the Cauchy stress tensor. We have scaled velocities with the first swimming mode B_1, lengths with the squirmer radius a, time with the convective time scale a/B_1 and stresses with $\mu_0 B_1/a$, where μ_0 is the total zero-shear viscosity of the fluid. The Reynolds number is given by $Re = \rho B_1 a/\mu_0$ where ρ is the fluid density. Owing to their small size and the viscous environments in which they are commonly found, microorganisms swim at virtually zero Reynolds number (Purcell 1977). Thus, we assume Stokes flow ($Re = 0$) for our asymptotic theory, and conduct our numerical simulations at sufficiently low Re such that the kinematics are not significantly affected by inertia; we find $Re = 0.1$ to be sufficient for these purposes.

For a viscoelastic fluid, the total stress $\boldsymbol{\sigma}$ can be expressed as

$$\boldsymbol{\sigma} = -p\boldsymbol{I} + \beta(\nabla\boldsymbol{u} + \nabla\boldsymbol{u}^T) + \boldsymbol{\tau}^p, \tag{2.3}$$

where $\boldsymbol{\tau}^p$ is the polymer extra-stress tensor and $\beta = \mu_s/(\mu_s+\mu_p) = \mu_s/\mu_0$ is the viscosity ratio for a fluid with solvent viscosity μ_s and polymer viscosity μ_p; $\boldsymbol{\tau}^p$ is

determined with the Giesekus constitutive model (Giesekus 1982)

$$\boldsymbol{\tau}^p = \frac{1-\beta}{Wi}(\boldsymbol{c}-\boldsymbol{I}) \tag{2.4}$$

$$Wi\,\overset{\triangledown}{\boldsymbol{c}} + (\boldsymbol{c}-\boldsymbol{I}) + \alpha_m(\boldsymbol{c}-\boldsymbol{I})^2 = 0. \tag{2.5}$$

In (2.4) and (2.5), $\boldsymbol{c}$ is the polymer conformation tensor, $\overset{\triangledown}{\boldsymbol{c}} = \partial\boldsymbol{c}/\partial t + \boldsymbol{u}\cdot\nabla\boldsymbol{c} - \nabla\boldsymbol{u}^T\cdot\boldsymbol{c} - \boldsymbol{c}\cdot\nabla\boldsymbol{u}$ is the upper-convected time derivative, and $Wi = \lambda B_1/a$ is the Weissenberg number, which describes the degree of fluid elasticity. The Giesekus constitutive equation considers the polymer molecules in the fluid to be Hookean dumbbells, and allows for anisotropic drag on these dumbbells via the Giesekus mobility parameter α_m (Bird, Armstrong & Hassager 1977).

3. Solution methodology

3.1. *Numerical solution*

We numerically solve the above set of equations as follows. We consider the co-moving frame of reference, i.e. the stationary squirmer experiences a uniform flow given by $-U\boldsymbol{e}_z$. This uniform flow is imposed on the outer walls of a cylindrical domain with length $40a$ and radius $20a$. This simulation set-up is shown in figure 1(a). This uniform flow is also specified at the inlet (top) of the box, where additionally the conformation tensor is set to identity, $\boldsymbol{c} = \boldsymbol{I}$. A convective outlet boundary condition is used at the exit of the simulation box.

As a minimal model for a squirmer with swirl, we consider the slip velocity given by (2.1) with the first two polar modes (corresponding to B_1 and B_2) and the second azimuthal mode (corresponding to C_2) as being non-zero. Thus, in the chosen frame of reference, the boundary condition at the surface of the squirmer is

$$\boldsymbol{u}|_{r=1} = \left(\sin(\theta) + \frac{\xi}{2}\sin(2\theta)\right)\boldsymbol{e}_\theta + \left(\Omega\sin(\theta) + \frac{3\zeta}{2}\sin(2\theta)\right)\boldsymbol{e}_\phi. \tag{3.1}$$

As previously discussed, $\xi = B_2/B_1$ denotes the type of swimmer: pushers have $\xi < 0$, pullers have $\xi > 0$ and 'neutral' squirmers have $\xi = 0$. The new dimensionless group $\zeta = C_2/(B_1a^3)$ denotes the relative magnitude of the azimuthal to the polar flow around the swimming organism. The reason we consider the C_2 swirling mode, corresponding to a rotlet dipole flow (Pak & Lauga 2014), is to produce in a simple way the flow field of a microorganism with a rotating flagellum and counter-rotating body. To illustrate this flow qualitatively, in figure 1(b), we visualize streamlines around a neutral squirmer ($\xi = 0$) for $\zeta = 5$ and $Wi = 0$.

We solve the above governing equations and boundary conditions using a third-order accurate finite volume flow solver developed by Stanford's Center for Turbulence Research (Ham, Mattsson & Iaccarino 2006). Equation (2.5) is solved as six scalar equations (since $\boldsymbol{c}$ is symmetric) using a log-conformation approach to ensure $\boldsymbol{c}$ remains positive–definite (Fattal & Kupferman 2004; Hulsen, Fattal & Kupferman 2005). Further details of the method described thus far, including extensive validation studies and comparison with experiments, can be found in previously published works (Richter, Iaccarino & Shaqfeh 2010; Padhy *et al.* 2013; Yang, Krishnan & Shaqfeh 2016; Castillo *et al.* 2019). Since a microorganism swimming at low Reynolds number must be force and torque free (Lauga & Powers 2009), we iteratively calculate U and Ω through time stepping until the

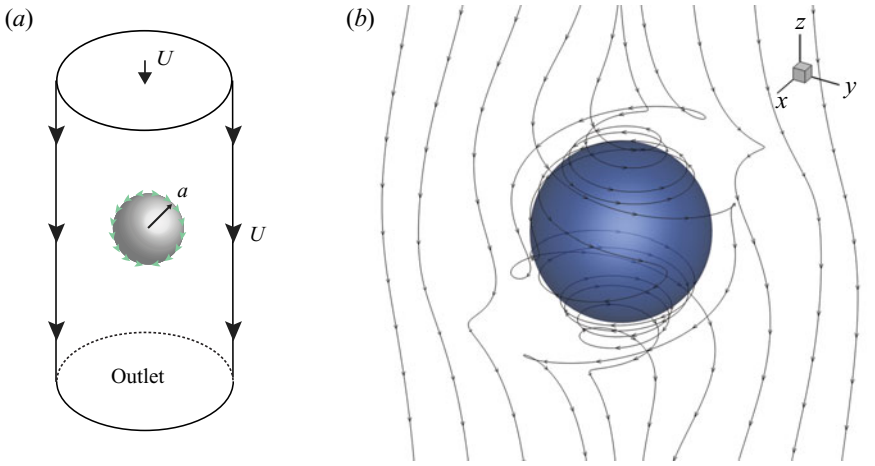

FIGURE 1. (*a*) Simulation set-up for a squirmer with swirl as seen in the co-moving frame (swimming in the positive z direction). Note that the dimensions are not drawn to scale. (*b*) Streamlines around the neutral squirmer (ξ) at $Wi = 0$ and $\zeta = 5$, shown to illustrate the qualitative shape of the flow that results from the inclusion of the term related to azimuthal swirl in (3.1).

z-components of the measured net force and torque on the squirmer vanish at steady state (the other components of force and torque vanish due to the axisymmetry of the problem). Since we work in the co-moving frame of reference, it is natural to use a body-fitted mesh; thus we make use of an unstructured mesh of tetrahedral elements with increasing resolution near the squirmer. We have conducted a series of studies on successively refined meshes in space and time to ensure the accuracy of our simulations; the kinematic results presented change by no more than 1 % when moving to a mesh size or time step size that is two times as coarse.

3.2. *Asymptotic solution*

We augment our simulations with an asymptotic theory valid in the limit of $Wi \ll 1$. Specifically, we consider a regular perturbation expansion to obtain U and Ω as a power series in Wi. The theoretical analysis is performed using (2.2), (2.3) and (2.5) for zero Reynolds numbers ($Re = 0$), an unbounded flow, and assuming steady state. Because of the particle geometry, the equations are expressed conveniently in a spherical coordinate system $r\theta\phi$ where r is the distance from the centre of the particle, θ is the polar angle ($0 \leq \theta \leq \pi$) and ϕ is the azimuthal angle ($0 \leq \phi < 2\pi$). The domain of definition of the governing equations is $\boldsymbol{D} = \{1 < r < \infty,\ 0 < \theta < \pi,\ 0 \leq \phi < 2\pi\}$. Although all the components of the velocity are non-zero, the flow is axisymmetric, i.e. there is no dependence of the dependent flow variables on ϕ:

$$p = p(r,\theta),\quad \boldsymbol{u} = \sum_{i=r,\theta,\phi} u_i(r,\theta)\,\boldsymbol{e}_i,\quad \boldsymbol{\tau}^p = \sum_{i,j=r,\theta,\phi} \tau^p_{i,j}(r,\theta)\,\boldsymbol{e}_i\boldsymbol{e}_j,\quad \boldsymbol{c} = \sum_{i,j=r,\theta,\phi} c_{i,j}(r,\theta)\,\boldsymbol{e}_i\boldsymbol{e}_j. \tag{3.2a–d}$$

Note that $\boldsymbol{\tau}^p$ and $\boldsymbol{c}$ are connected linearly (see (2.4) above). In the spherical coordinate system, the boundary conditions on the surface of the particle are

$$u_r = 0,\quad u_\theta = \sin(\theta) + \frac{\xi}{2}\sin(2\theta),\quad u_\phi = \Omega\sin(\theta) + \frac{3}{2}\zeta\sin(2\theta)\quad \text{at } r = 1. \tag{3.3}$$

The above conditions in conjunction with the continuity equation give

$$\left.\frac{\partial u_r}{\partial r}\right|_{r=1} = -\frac{\xi}{2} - 2\cos(\theta) - \frac{3\xi}{2}\cos(2\theta). \tag{3.4}$$

Far from the particle, the far-field flow is given as

$$u_r^{\infty} = -U\cos(\theta), \quad u_\theta^{\infty} = U\sin(\theta), \quad u_\phi^{\infty} = 0, \quad p^{\infty} = 0, \tag{3.5a–d}$$

where the superscript ∞ denotes value at infinity ($r \to \infty$).

The unknown far-field flow velocity, U, and rotation rate of the particle, Ω, are determined by ensuring the microswimmer is force and torque free (Lauga & Powers 2009)

$$\int_{r=1} \boldsymbol{e}_r \cdot \boldsymbol{\sigma}\, \mathrm{d}S = \boldsymbol{0}, \quad \int_{r=1} \boldsymbol{e}_r \times (\boldsymbol{e}_r \cdot \boldsymbol{\sigma})\, \mathrm{d}S = \boldsymbol{0}. \tag{3.6a,b}$$

The non-trivial components of the force-free condition (FFC) and the torque-free condition (TFC) are, respectively,

$$\int_0^{\pi} \left\{ \left(\frac{p}{2}\sin(2\theta)\right) + \beta\left(\left(\frac{1}{r}\frac{\partial u_r}{\partial \theta} + \frac{\partial u_\theta}{\partial r} - \frac{u_\theta}{r}\right)\sin^2(\theta) - \frac{\partial u_r}{\partial r}\sin(2\theta)\right) + \left(\tau_{r\theta}^p \sin^2(\theta) - \tau_{rr}^p \frac{\sin(2\theta)}{2}\right)\right\} \mathrm{d}\theta = 0 \tag{3.7}$$

$$\int_0^{\pi} \left(\beta\left(\frac{\partial u_\phi}{\partial r} - \frac{u_\phi}{r}\right) + \tau_{r\phi}^p\right)\sin^2(\theta)\, \mathrm{d}\theta = 0. \tag{3.8}$$

Although (3.7) and (3.8) are evaluated at $r = 1$ in order to determine U and Ω, one can prove that, under steady state and creeping conditions, they hold at any radial position, $r \geq 1$. Finally, note that with the asymptotic analysis, no boundary conditions are applied (and cannot be imposed) for the polymer extra stress $\boldsymbol{\tau}^p$.

In order to solve (2.2), (2.3) and (2.5) accompanied by the auxiliary conditions ((3.3) to (3.5) and (3.8) and § 3.2), we use a regular perturbation scheme in terms of the Weissenberg number. In particular, for a weakly viscoelastic fluid, i.e. $0 < Wi << 1$, the solution for all the dependent variables is given as a standard power series expansion in terms of Wi

$$\left.\begin{array}{c} X \approx X_0 + Wi\, X_1 + Wi^2\, X_2 + \cdots \\ X = U,\, \Omega,\, p,\, u_r,\, u_\theta,\, u_\phi,\, \tau_{rr}^p,\, \tau_{\theta\theta}^p,\, \tau_{r\theta}^p,\, \tau_{\phi\phi}^p,\, \tau_{r\phi}^p,\, \tau_{\theta\phi}^p \end{array}\right\}, \tag{3.9}$$

where the zero-order term, X_0, corresponds to the simple Newtonian fluid. In this type of analysis, the remaining parameters a_m, β, ζ, ξ are considered $O(1)$ quantities. The solution procedure for a similar flow problem with no-slip boundary conditions has been described in recent work by Housiadas (2019) and the interested reader is referred thereto for more details.

The analytical solution for the Newtonian fluid, i.e. for the Stokes equations, is

$$u_{r,0} = \frac{\xi}{4}\left(\frac{1}{r^4} - \frac{1}{r^2}\right)(1 + 3\cos(2\theta)) + U_0\left(\frac{1}{r^3} - 1\right)\cos(\theta), \tag{3.10}$$

$$u_{\theta,0} = U_0\left(1 + \frac{1}{2r^3}\right)\sin(\theta) + \frac{\xi}{2r^4}\sin(2\theta), \tag{3.11}$$

$$u_{\phi,0} = \frac{\Omega_0}{r^2}\sin(\theta) + \frac{3\zeta}{2r^3}\sin(2\theta), \tag{3.12}$$

$$p_0 = -\frac{\xi}{2r^3}(1 + 3\cos(2\theta)). \tag{3.13}$$

Note that $U_0 = \frac{2}{3}$ and $\Omega_0 = 0$ have been determined. We have also solved the perturbation equations analytically up to $O(Wi^4)$ using the 'Mathematica' software (Wolfram Research, Inc. 2019). The most important results are the velocity at infinity and the rotation rate of the swimmer. We find

$$U \approx \frac{2}{3} + (1-\beta)\,Wi\left(U_1 + Wi\,U_2 + Wi^2\,U_3 + Wi^3\,U_4\right), \tag{3.14}$$

where U_1 and U_2, respectively, are

$$U_1 = \frac{2}{15}(\alpha_m - 1)\xi \tag{3.15}$$

$$\begin{aligned} U_2 = {} & \left(-\frac{772}{2145} - \frac{64\alpha_m}{65} + \frac{128\alpha_m^2}{195}\right) \\ & + \xi^2\left(-\frac{6218}{15015} - \frac{101168a_m}{45045} + \frac{7376a_m^2}{5005} + \left(-\frac{58}{1365} + \frac{3032a_m}{45045} - \frac{86a_m^2}{3465}\right)(1-\beta)\right) \\ & + \zeta^2\left(\frac{468}{385} - \frac{21744\alpha_m}{5005} + \frac{15744a_m^2}{5005} + \left(-\frac{4392}{5005} + \frac{1944a_m}{1001} - \frac{5328a_m^2}{5005}\right)(1-\beta)\right). \end{aligned} \tag{3.16}$$

For the rotation rate of the particle, we have found the solution up to fifth order in Wi

$$\Omega \approx \zeta\,Wi(1-\beta)\left(\Omega_1 + Wi\,\Omega_2 + Wi^2\,\Omega_3 + Wi^3\,\Omega_4 + Wi^4\,\Omega_5\right), \tag{3.17}$$

where Ω_1 and Ω_2 are given below.

$$\Omega_1 = \frac{6}{5}(1 - \alpha_m), \tag{3.18}$$

$$\Omega_2 = \xi\,\frac{12(1043 + 2912\alpha_m - 2000\alpha_m^2) - 6(623 - 1158\alpha_m + 535\alpha_m^2)(1-\beta)}{5005}. \tag{3.19}$$

The higher-order corrections for U and Ω are available upon request. Note that setting $\zeta = 0$ and $\beta = 0$ recovers the solution of Datt & Elfring (2019, 2020) through $O(Wi^3)$.

4. Results and discussion

4.1. *The effect of azimuthal swirl on the swimming speed*

We begin by looking at the effect of azimuthal swirl on the kinematics of the swimmer. Note that, while the rotation rate for our particular swimming gait is zero in a Newtonian fluid and under creeping flow conditions ($Re = 0$), i.e. $\boldsymbol{\Omega}_N = -C_1\boldsymbol{e}_z/a^3$ as given by Pak & Lauga (2014), it is actually non-zero but small ($\Omega \leq 0.25$) for finite Wi due to the nonlinear coupling between rotation and translation in a viscoelastic fluid (Castillo *et al.* 2019). Interestingly enough, the effect of this coupling on rotation rate even vanishes in the presence of significant fluid elasticity. We illustrate this in figure 2(*b*), where we plot the rotation rate scaled by its dominant scaling (as found in the previous section) for the case of a neutral squirmer. From this plot we see that there will only be a slight rotation due to the azimuthal swirl solely for small but finite Wi (i.e. $0.1 \lessapprox Wi \lessapprox 1$). Because of this, we will focus our attention on the change in translational speed for the remainder of this report. Unless otherwise stated, we will consider $\beta = 0.5$ and $\alpha_m = 0.2$ for the rheological properties of the fluid.

We first recall the effect of elasticity for the case of no swirl, where it was found that squirmers swim slower in a viscoelastic fluid for all Wi (Zhu *et al.* 2011, 2012). This result corresponds to the case of $\zeta = 0$ in figure 2, where we plot the swimming speed of the neutral squirmer ($\xi = 0$) normalized by the Newtonian swimming speed U_N as a function of Wi and ζ. Our results for $\zeta = 0$ differ by no more than 2.8 % from those of Zhu *et al.* (2012), serving as one validation of our current results. Without loss of generality we consider only positive ζ since changing its sign does not alter its effect on U from symmetry. For the cases of zero ($\zeta = 0$) or relatively small ($\zeta = 1$) azimuthal swirl we see that the squirmer swims slower in a viscoelastic fluid than it does in a Newtonian fluid. In stark contrast, for significant swirling flow ($\zeta = 3, 5$), the normalized speed exceeds unity indicating speed enhancement. Increasing Wi causes the effect to become more pronounced before appearing to reach an asymptotic value at large Wi. For all values of ζ, our numerical results are corroborated by the asymptotic theory (shown as dashed curves, cf. figures 2*a* and 3*a*) for small Wi, i.e. (3.14). The reason the agreement of the numerical solution with the asymptotic results is good only for small Wi is the strongly nonlinear character of the swirling slip velocity with viscoelasticity. It is also an indication of a coil–stretch transition at a finite Weissenberg number Wi_c, a case that does not allow for accurate predictions of the flow close to Wi_c using high-order perturbations methods (Housiadas 2017).

As mentioned in § 2.1, we nominally perform our simulations at a Re small enough such that the effect of inertia is minimized. We have also performed an additional set of simulations whereby we solved (2.2) only after completely discarding the second term, which represents convective forces in the fluid. In this way, we can carefully examine the impact inertia has in regards to creating a speed enhancement. These simulations are shown for the case of a neutral squirmer with swirl ($\zeta = 3, 5$) in figure 3(*b*). From this figure, we see that at most the error in retaining all terms of the Navier–Stokes equation is approximately 7 % (seen at the largest value of $Wi = 3$ and $\zeta = 5$). For smaller ζ, the difference is reduced to a few percentage points; indeed, one expects the difference in these two solution methodologies to vanish as ζ decreases since ζ controls the relative amount of rotational inertia in the fluid. An additional conclusion to be made from figure 3(*b*) is that the nonlinear rotational–translational coupling originating from fluid inertia (rather than fluid elasticity) appears to act synergistically with the latter to further increase the swimming speed. Since we are primarily interested in this work in the

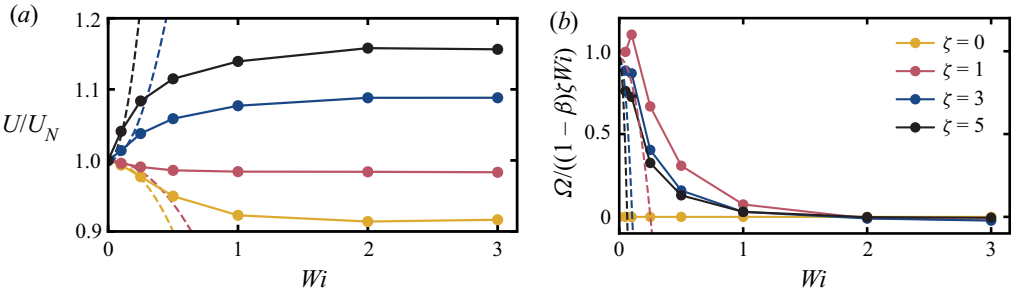

FIGURE 2. (*a*) Normalized swimming speed (U/U_N) and (*b*) scaled rotation rate as a function of Wi and ζ for the neutral squirmer ($\xi = 0$). Filled circles refer to numerical simulations while dashed lines refer to the asymptotic theory through $O(Wi^2)$ for U and through $O(Wi^3)$ for Ω. The results are presented in this way since only even (odd) terms with respect to Wi are non-zero in the asymptotic expansion for U (Ω) for the neutral squirmer. For significant swirl ($\zeta = 3, 5$), the squirmer swims faster in the viscoelastic fluid, with the speed increase growing with increasing fluid elasticity (Wi).

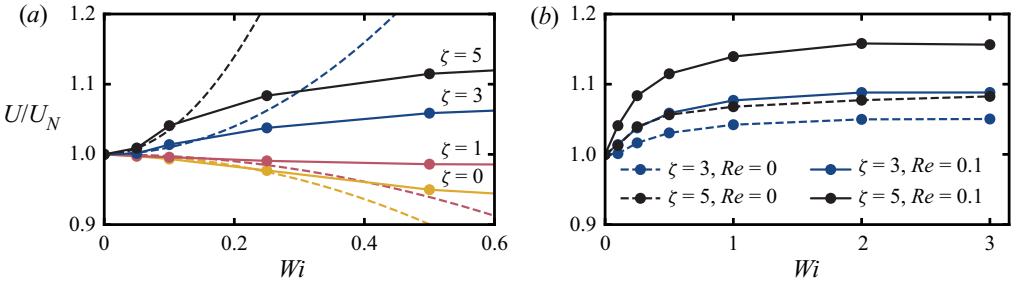

FIGURE 3. Normalized swimming speed (U/U_N) as a function of Wi and ζ for the neutral squirmer ($\xi = 0$). In (*a*) we recapitulate the results of figure 2(*a*) to better visualize the trends at low Wi. Dashed lines refer to the $O(Wi^2)$ solutions. In (*b*) we examine how the results change in the presence and absence of inertia ($Re = 0.1$ and 0, respectively). The latter ($Re = 0$) results were obtained by solving (2.2) after discarding the nonlinear convective term.

coupling originating from fluid elasticity rather than inertia, all subsequent simulations where we expect rotational inertia to be significant (i.e. $\zeta \geq 3$) are conducted at $Re = 0$ unless stated otherwise. In this way, our simulation results will present a lower bound on the effect of swirl in a viscoelastic fluid since any real swimming microorganism will experience some finite amount of inertia.

4.2. *The relationship between speed enhancement and the polymer stress in the surrounding flow*

To better understand the origin of the speed enhancement seen in figure 2, we examined the polymer stress field around the neutral squirmer in the case of no azimuthal swirl ($\zeta = 0$) and a significant degree of swirl ($\zeta = 5$) in figure 4. In figure 4, we are viewing the $y = 0$ plane for a swimmer moving in the positive z-direction. We first look at the z–z component of the polymer stress tensor, shown in figure 4(*a*) as a function of ζ. It is seen that the large amount of extensional stress in the swimmer's wake in the case of no swirl diminishes dramatically in the presence of significant swirling flow. This follows

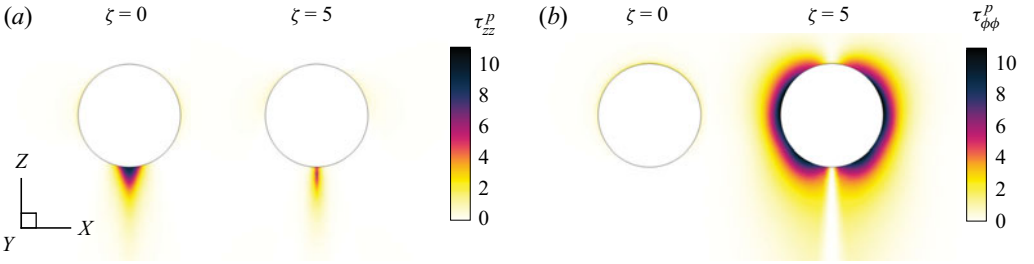

FIGURE 4. Components of the polymer stress tensor ($\boldsymbol{\tau}^p$) surrounding the neutral squirmer (swimming in the positive z direction) at $Wi = 2$. (*a*) The z–z component of the polymer stress (τ_{zz}^p) is largest behind the swimmer and diminishes once swirl is introduced ($\zeta = 5$). (*b*) In contrast, the ϕ–ϕ component of the polymer stress ($\tau_{\phi\phi}^p$) is essentially non-existent in the case of no swirl ($\zeta = 0$) and becomes the dominant component of the polymer stress tensor at $\zeta = 5$.

since for no swirl the back of the swimmer is an extensional point in the flow field, where polymers can readily deform and cause marked decrease in swimming speeds (Shen & Arratia 2011; Binagia *et al.* 2019). By changing the slip velocity to include an azimuthal component, we necessarily introduce a vortical component to the flow near this location, thereby decreasing its extensional character. With the diminution of extensional stress, we see the creation of hoop stresses (corresponding to $\tau_{\phi\phi}^p$ in spherical coordinates) when azimuthal swirl is included in the model (cf. figure 4*b*). Note that this is the type of stress alluded to by Patteson *et al.* (2015), who hypothesized that hoop stresses could decrease cell wobbling and thereby lead to straighter swimming trajectories and consequently faster speeds.

These trends for the polymer stress suggest a possible mechanisms for the speed enhancement seen in figure 2. As the large extensional τ_{zz}^p stress found behind the swimmer in the case of no swirl ($\zeta = 0$) was previously reported to be responsible for speed hindrance (Zhu *et al.* 2012), we expect its diminution to lead to an increase in the swimming speed.

To examine this hypothesis in more detail we consider the force tractions acting on the surface of the swimming microorganism. The net force acting on the particle in the swimming direction is given in indicial notation by $F_z = \int_S \sigma_{zj} n_j \, \mathrm{d}S = 0$. This net force can be decomposed into pressure, viscous and polymeric contributions according to (2.3): i.e. $F_z = F_z^{pres} + F_z^{visc} + F_z^{poly} = 0$. We plot each of these contributions to the net force in figure 5 as a function of Wi for $\zeta = 0$ and $\zeta = 5$. We also further decompose the polymer contribution into that related to the normal stress τ_{zz}^p and the shear stress $\tau_{z\rho}^p$ (where ρ refers to the radial coordinate in cylindrical coordinates). That is, $F_z^{poly} = \int_S \tau_{zz}^p n_z \, \mathrm{d}S + \int_S \tau_{z\rho}^p n_\rho \, \mathrm{d}S$ (with no contribution related to $\tau_{z\phi}^p$ since $n_\phi = 0$). We see from figure 5 that the inclusion of azimuthal swirl (i.e. moving from figures 5*a* to 5*b*) only causes a slight change in the contribution related to the polymer shear stress $\tau_{z\rho}^p$. In contrast, the presence of swirl significantly affects the normal stress (τ_{zz}^p) contribution to the net force, causing it to not only increase but actually become propulsive for all Wi. This trend can be anticipated from figure 4(*a*), where the inclusion of swirl removes the region of high extensional resistance behind the swimmer but does not significantly change the small regions located at the front half of the swimmer that yield positive contributions to the net force.

To better visualize this, in figure 6 we plot the surface tractions related to τ_{zz}^p and $\tau_{z\rho}^p$ as a function of the polar angle θ. We immediately see that the biggest change with the

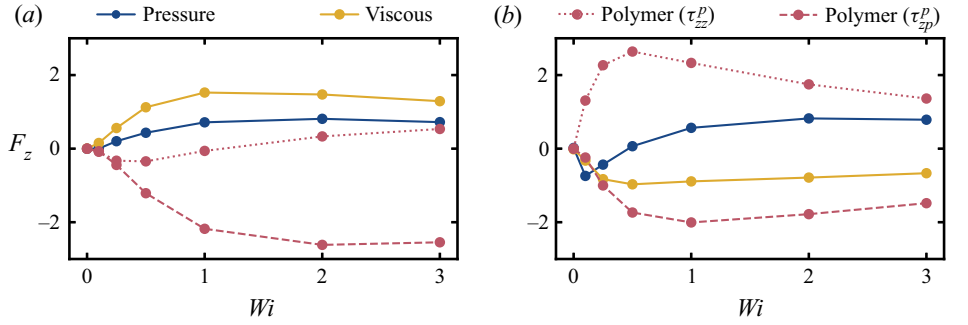

FIGURE 5. Net force contributions acting in the swimming (z) direction in the case of (a) $\zeta = 0$ and (b) $\zeta = 5$. The pressure, viscous and polymer contributions are given in cylindrical coordinates by $F_z^{pres} = -\int_S p n_z \,\mathrm{d}S$, $F_z^{visc} = \beta \int_S (\nabla_z u_j + \nabla_j u_z) n_j \,\mathrm{d}S$ and $F_z^{poly} = \int_S \tau^p_{zj} n_j \,\mathrm{d}S$, respectively (i.e. $F_z = F_z^{pres} + F_z^{visc} + F_z^{poly} = 0$). The polymer stress contribution, F_z^{poly}, is further broken down into portions related to normal polymeric stresses (τ^p_{zz}) and shear polymeric stresses ($\tau^p_{z\rho}$); notably, the former becomes positive (acting as a thrust) for all Wi in the presence of significant swirl ($\zeta = 5$).

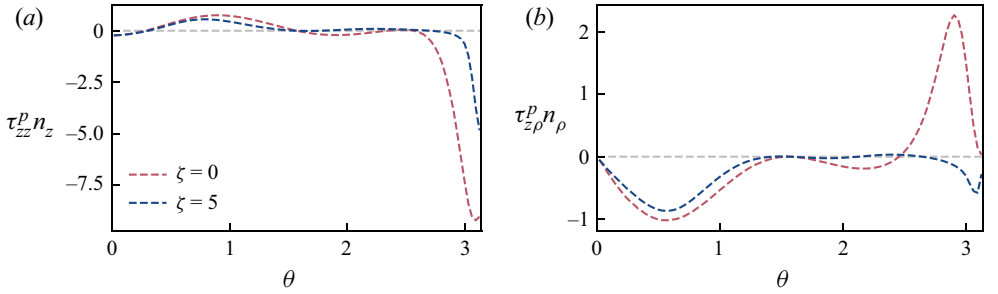

FIGURE 6. Surface tractions (a) $\tau^p_{zz} n_z$ and (b) $\tau^p_{z\rho} n_z$ as a function of the polar angle θ and the degree of azimuthal swirl, ζ, for a neutral squirmer at $Wi = 2$. With increasing swirl, $\tau^p_{zz} n_z$ degrees in magnitude near the back of the squirmer ($\theta = \pi$). In contrast, $\tau^p_{z\rho} n_z$ increases with increasing ζ for most values of θ, except near $\theta = \pi$ where it decreases significantly and actually changes sign.

addition of swirl occurs at the back of the swimmer, i.e. near $\theta = \pi$. Notably, $\tau^p_{zz} n_z$, which nominally is responsible for the slow down in the case of no swirl (Zhu *et al.* 2012), severely decreases in magnitude as ζ is increased. All else equal, one would expect this to lead to an increase in the swimming speed. Of course the net effect depends on how the surface tractions related to the hoop stresses, i.e. $\tau^p_{z\rho} n_\rho$, vary with ζ. From figure 6(b), we that while there is an increase of $\tau^p_{z\rho} n_\rho$ for most values of θ in the presence of swirl, a significant decrease is seen near $\theta = \pi$. These two trends appear to offset each other; this explains the minimal change in the component of F_z related to $\tau^p_{z\rho}$ seen in figure 5. We thus argue that it is the change in the extensional stress that dominates the change in speed. Thus, taking the results of figures 4 to 6 together, we conclude that the microswimmer experiences an increase in its swimming speed when the rotational flow originating from the rotlet dipole squirming mode is significant enough to disrupt the predominantly extensional flow behind the squirmer.

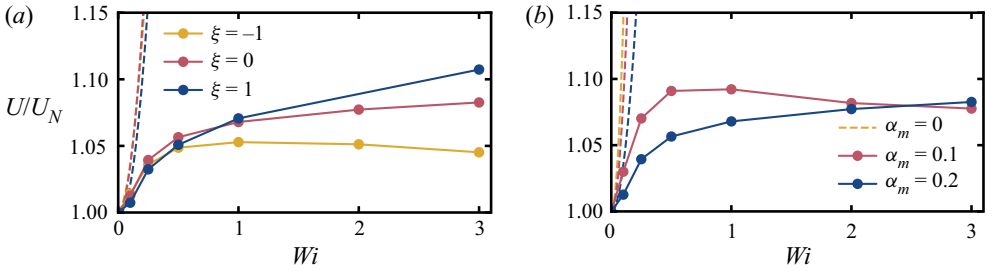

FIGURE 7. Normalized swimming speed (U/U_N) as a function of fluid elasticity (Wi), swimmer type (ξ) and fluid rheology (α_m) in the case of significant swirl ($\zeta = 5$). Filled circles refer to numerical simulations while dashed lines refer to the asymptotic theory through $O(Wi^2)$.

4.3. *The effect of the swimmer type (ξ) and Giesekus mobility parameter (α_m)*

We would now like to examine how robust the results seen in figure 2 (namely the speed enhancement for significant azimuthal swirl) are to changes in the swimmer type and the degree of shear-thinning present in the viscoelastic fluid (tuned via the Giesekus mobility parameter α_m). In figure 7 we plot the normalized swimming speed for a pusher ($\xi = -1$), a puller ($\xi = 1$), and a neutral squirmer ($\xi = 0$) as a function of Wi at $\zeta = 5$. We see that the effect of swimming type is modest; pullers exhibit a slightly more pronounced speed enhancement than that of neutral squirmers while the effect is diminished for pushers. This makes sense in light of the results of Zhu *et al.* (2012), where it was found that the pusher had the greatest region of extensional stress behind the swimmer by a large margin when compared with that of the other swimmer types. Given the mechanism we described in the preceding paragraph, we therefore expect the pusher to experience a smaller speed increase compared with the other swimmer types in the presence of significant swirl given that there is a greater degree of extensional resistance in the wake to overcome.

In figure 7(*b*) we plot the normalized swimming speed for the neutral squirmer ($\xi = 0$) as a function of Wi and the Giesekus mobility parameter (α_m). Note that, in the limit of $\alpha_m = 0$, the Oldroyd-B model is recovered, which does not exhibit shear thinning (Giesekus 1982). Thus, decreasing α_m amounts to systematically removing shear thinning from the predictions of the constitutive model for pure shearing. Interestingly, we see from figure 7(*b*) that the speed enhancement seen in figure 2 for $\alpha_m = 0.2$ actually becomes more pronounced as α_m is decreased for all but the largest value of $Wi = 3$. We explore this effect further in figure 8, where we examine the swimming speed for a neutral squirmer with significant swirl ($\xi = 0$, $\zeta = 5$) at $Wi = 0.5$ as a function of α_m. We see that as α_m approaches zero, both theory (specifically, the diagonal Padé [2/2] approximant of (3.14); Housiadas 2017) and simulation predict an increase in the normalized speed. This suggests that the effect of shear thinning is to diminish the enhancement in speed created by the swirling flow; additionally, it means that the results presented at $\alpha_m = 0.2$ effectively serve as a conservative estimate of the amount by which the swimming speed will be enhanced in a viscoelastic fluid. Thus, after examining figures 7(*b*) and 8, we believe the mechanism for speed enhancement is not related to the fluid thinning around the swimming microorganism but is rather solely related to the elasticity of the surrounding fluid.

The other rheological parameter that remains to be explored is the viscosity ratio β. In figure 9 we examine the effect of β for a neutral squirmer exhibiting a significant degree of swirl, $\zeta = 5$. Starting from a Newtonian fluid ($\beta = 1$), it appears that the

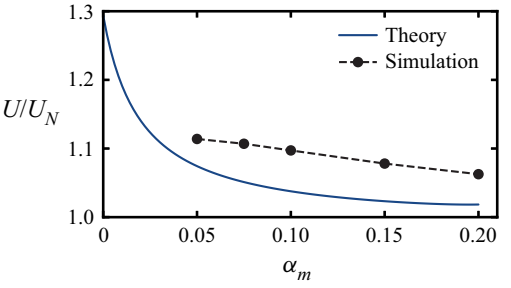

FIGURE 8. Normalized swimming speed (U/U_N) as a function of the Giesekus mobility parameter (α_m) for a neutral squirmer ($\xi = 0$) with significant swirl ($\zeta = 5$) at $Wi = 0.5$. Both the Padé [2/2] approximant of the asymptotic theory (blue, solid line) and numerical simulations (black, dashed line) predict a further enhancement in speed as α_m tends to zero, indicating that the value of $\alpha_m = 0.2$ chosen for the majority of this study is a conservative estimate for the effect of swirl on speed.

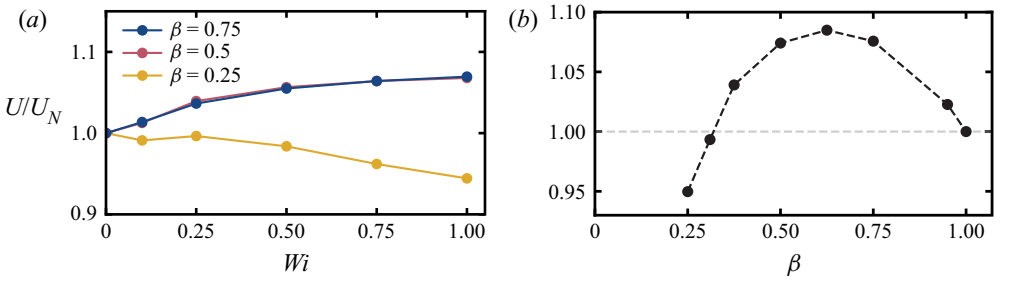

FIGURE 9. Normalized swimming speed (U/U_N) for the neutral squirmer ($\xi = 0$) having a significant degree of azimuthal swirl ($\zeta = 5$) (*a*) as a function of *Wi* for discrete values of β and (*b*) as a function of β at $Wi = 1$.

normalized swimming speed is greater than unity for all *Wi* for β as low as 0.5. As β is decreased further (i.e. larger fraction of polymer in solution), there comes a critical value of the viscosity ratio where the normalized speed actually becomes less than 1 for all *Wi*. Intuitively, this makes sense, since as β decreases we expect the viscoelastic wake seen in figure 4(*a*) (which nominally leads to a decrease in the swimming speed) to become more pronounced. This non-monotonic trend with respect to β can also be seen in figure 9(*b*), where we plot the normalized swimming speed at $Wi = 1$, $\zeta = 5$, $\xi = 0$ for a range of β. From this figure we see that the swimming speed increases from unity until a maximum speed enhancement is reached near $\beta = 0.625$ for this value of *Wi*. Past this value, decreasing β leads to a speed decrease until the normalized speed becomes less than one for sufficiently small viscosity ratios.

4.4. *Estimating ζ and ξ for a real swimming microorganism*

Could the phenomenon observed in this paper be responsible for the recent observation that *E. coli* swims faster in a viscoelastic fluid (Patteson *et al.* 2015)? To assess the relative significance of the azimuthal flow created by *E. coli*'s rotating flagellum and counter-rotating body, we would like to estimate ξ and ζ for a typical swimming *E. coli*. In regards to $\xi = B_2/B_1$, B_1 is set via the Newtonian swimming speed since $U_N = \frac{2}{3}B_1$

(Lighthill 1952; Blake 1971), where $U_N = 8.3\ \mu\text{m s}^{-1}$ (Patteson *et al.* 2015), and B_2 is calculated via the experimentally measured dipole strength of *E. coli* (Drescher *et al.* 2011). We do so by comparing the analytical expression for the far-field disturbance flow of the squirmer (Ishikawa *et al.* 2006) to the experimentally measured force dipole flow of *E. coli* (Drescher *et al.* 2011), giving an estimate of $B_2 \approx -3.5\ \mu\text{m s}^{-1}$ and thus $\xi \approx -0.28$, which is well within the regime considered in figure 2. To calculate $\zeta = C_2/(a^3 B_1)$, we estimate C_2/a^3 by relating the linear velocity of *E. coli*'s rotating helix (rotating at 100 Hz and having a helical diameter of 0.5 μm (Lauga 2016)) to the average azimuthal velocity on the back half of the squirmer. We find that $\zeta = C_2/(a^3 B_1) \approx 4.2$, indicating that the effect of azimuthal swirl should be quite significant for *E. coli* swimming in an elastic fluid given the results seen in figure 2.

4.5. *The effect of changing the fluid constitutive equation*

A natural question at this point is how robust the prior results (e.g. figure 2) are to the particular choice of polymer constitutive equation. To answer this, we have conducted simulations using the FENE-P model (Peterlin 1966) as opposed to the Giesekus model seen above. The FENE-P model defines the extra polymer stress in terms of $\boldsymbol{c}$ as

$$\boldsymbol{\tau}^p = \frac{1-\beta}{Wi}\left(\frac{\boldsymbol{c}}{\psi} - \boldsymbol{I}\right) \tag{4.1}$$

$$Wi\ \overset{\triangledown}{\boldsymbol{c}} + \left(\frac{\boldsymbol{c}}{\psi} - \boldsymbol{I}\right) = 0, \tag{4.2}$$

where $\psi = 1 - c_{ii}/L^2$ is the spring-stiffening function and c_{ii} is the trace of the conformation tensor. The FENE-P model considers polymer molecules to be dumbbells with a finite extensibility L. Thus, we see that for large L, $\psi \to 1$ and the FENE-P model reduces to the Oldroyd-B constitutive equation.

In figure 10(*a*), we examine the effect of swirl on the swimming speed of a neutral squirmer ($\xi = 0$) using the FENE-P model with $L = 5$. Note that for this value of L the maximum polymer stretch (i.e. c_{ii}) in the surrounding flow field nearly matches that measured for our previous results with the Giesekus model using $\alpha_m = 0.2$. For example, $\max c_{ii}$ (where the maximum is taken over the computational domain) differs by less than 2 % when comparing the pair of simulations using different constitutive models at $\zeta = 0$, $Wi = 1$. Still, from viewing figure 10(*b*), we see that increasing L only induces a slight quantitative change in the swimming speed for all Wi. Note that this range of L spans two orders of magnitude for ψ since it is the square of L that appears in the spring-stiffening function.

For small to intermediate values of Wi, the effect of swirl is as before (i.e. figure 2); increasing swirl (ζ) increases the swimming speed, even leading to a speed enhancement for large enough values of ζ. In contrast to the results seen using the Giesekus constitutive equation, we see a non-monotonic trend of U/U_N with respect to Wi for non-zero swirl. Notably, there appears to be a maximum speed enhancement observed near $Wi = 0.5$ before the normalized speed decreases monotonically at large Wi.

This result implies that qualitative differences can be seen for the effect of fluid rheology on the swimming kinematics if Wi is sufficiently large. Intuitively this is what we expect; at such large Wi the specific way in which the polymer stress is modelled will of course become more pronounced. It should be noted, though, that these values of Wi are unlikely to be seen for real swimming microorganisms. For example, in the work of Patteson

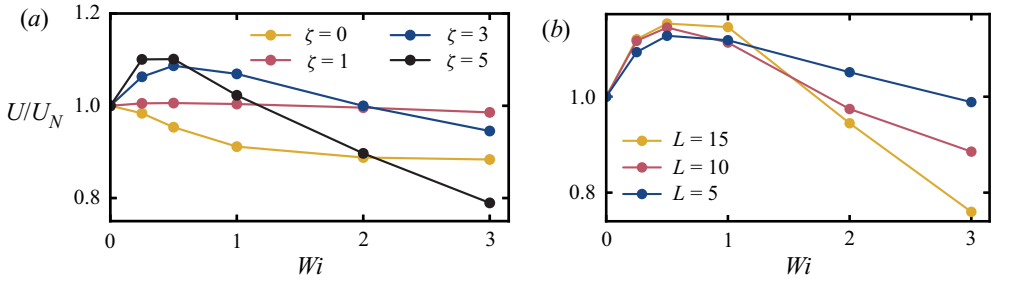

FIGURE 10. (*a*) Normalized swimming speed (U/U_N) as a function of Wi and ζ for the neutral squirmer ($\xi = 0$) using the FENE-P constitutive equation ($L = 5$, $\beta = 0.5$). (*b*) Normalized swimming speed as a function of Wi and L for a neutral squirmer with $\zeta = 3$ at $Re = 0.1$.

et al. (2015), the maximum mean cell velocity that they observed, 12.4 μm s^{-1}, occurs in their most elastic fluid, which has a relaxation time $\lambda = 3.96 \times 10^{-2}$. Thus a conservative estimate for Wi (using an effective length of the bacteria $l = 7$ μm) is $Wi = \lambda U_0/l \approx 0.07$. Note that our definition of Wi throughout this report defines $Wi = \lambda B_1/a$ for the squirmer model; $U \approx 2/3B_1$ at small Wi, so we conclude that $Wi \lessapprox 0.1$ is the relevant regime for microorganisms swimming in viscoelastic fluids. Thus for biologically relevant conditions, our model (regardless of the polymer model used) predicts a speed enhancement for swimmers creating a significant amount of azimuthal flow.

We would also like to examine how the choice of the polymer constitutive equation affects the force decomposition illustrated in figure 5. Interestingly enough, we see that analogous to figure 5, azimuthal swirl has little to no effect on the net force originating from the off-diagonal component of polymer stress, $\tau^p_{z\rho}$. In contrast, an increase of swirl from $\zeta = 0$ to $\zeta = 5$ is again associated with an increase in the net force related to τ^p_{zz} for all Wi. It is interesting to note that in contrast to that seen in figure 5, for the FENE-P model the viscous contribution to F_z is non-monotonic for $\zeta = 5$. In fact, the local minima for the viscous contribution in figure 11(*b*) occurs at the same Wi for which the maximum speed enhancement is observed (cf. figure 10). Taken together with figure 5, we see that the trends exhibited by the viscous net force are correlated to the normalized swimming speed. That is, $F_z^{visc} > 0$ appears to be associated with speed reduction while $F_z^{visc} < 0$ is indicative of speed enhancement.

4.6. *Hydrodynamic power and efficiency*

Finally, we would like to briefly discuss how the energy expenditure of a squirmer varies with the amount of azimuthal swirl present in its gait. The hydrodynamic power P and efficiency η are given by $P = -\int_S \boldsymbol{u} \cdot \boldsymbol{\sigma} \cdot \boldsymbol{n}\, \mathrm{d}S$ and $\eta = FU/P$, respectively, where F is the force required to tow a passive sphere of the same size as the squirmer at a constant speed U (Zhu *et al.* 2012). In figure 12, we plot each of these quantities, normalized by their values in a Newtonian fluid, P_N and η_N. We define P_N and η_N as the power and efficiency of a squirmer swimming in a Newtonian fluid that has the same gait (i.e. same value of ξ and ζ) as that under consideration (meaning P_N and η_N are themselves functions of ζ). In particular, P_N is given by $P_N = 2\pi(\frac{48}{5}\zeta^2 + \frac{4}{3}(2 + \xi^2))$. With the normalization suitably defined, we can see from figure 12(*a*) that the power expenditure for a given gait always decreases with increasing fluid elasticity, with the rate of this decrease proportional to the amount of azimuthal swirl present in swimmer's gait. Conversely, the efficiency increases with increasing Wi for each gait; the rate of this increase again proportional to

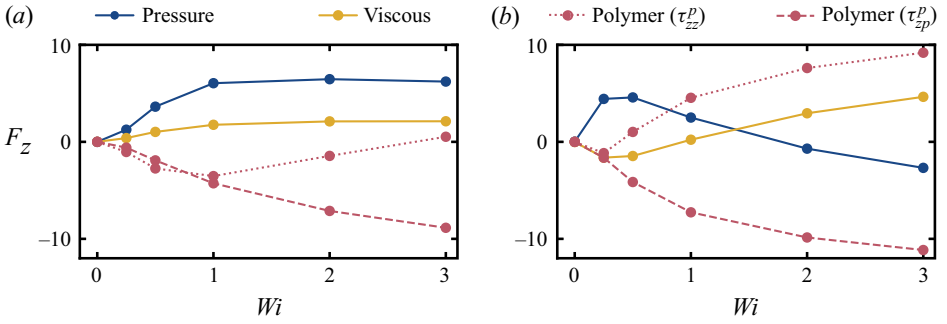

FIGURE 11. Net force contributions acting in the swimming (z) direction in the case of (a) $\zeta = 0$ and (b) $\zeta = 5$ when using the FENE-P constitutive equation ($L = 5$, $\beta = 0.5$). The polymer stress contribution, $F_z^{poly} = \int_S \tau_{zj}^p n_j \, \mathrm{d}S$, is broken down into portions related to normal polymeric stresses (τ_{zz}^p) and shear polymeric stresses ($\tau_{z\rho}^p$).

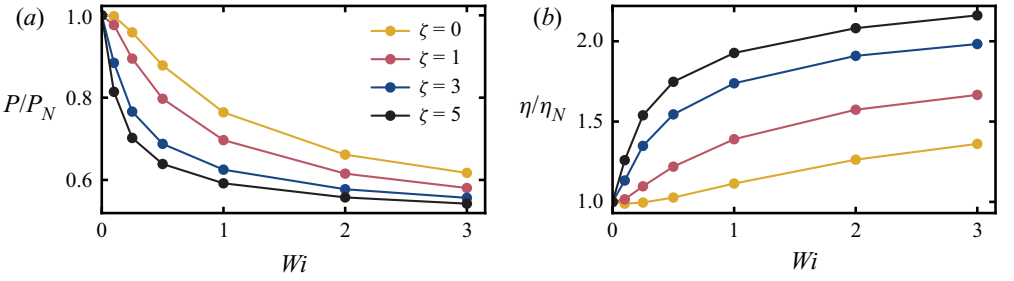

FIGURE 12. Normalized hydrodynamic power and efficiency as a function of Wi and degree of swirl, ζ, for a neutral squirmer ($\xi = 0$). P_N and η_N are defined as the power and efficiency at $Wi = 0$ for a squirmer with the same gait (i.e. value of ζ and ξ). (a) For all gaits, power decreases with increasing fluid elasticity; the rate of decreases increases with increasing azimuthal swirl. (b) Efficiency increases as a function of Wi for all gaits. The magnitude of this increase is in proportion to the amount of swirl present in the swimmer's gait.

the amount of swirl present. Note that each gait is more efficient in an elastic fluid than its Newtonian counterpart since $\eta/\eta_N > 1$ for every Wi and ζ. This implies that a swimmer with significant azimuthal swirl not only swims faster in a viscoelastic fluid but is also more energy efficient in its power expenditure than its Newtonian counterpart. It should be noted, however, that all else considered equal (e.g. holding Wi constant), increasing ζ leads to a monotonic increase in power expended. For example at $Wi = 0$, $P_N(\zeta = 0) \approx 0.22P_N(\zeta = 1) \approx 0.030P_N(\zeta = 3) \approx 0.011P_N(\zeta = 5)$. Thus, if we were to normalize all data in figure 12 by $P_N(\zeta = 0)$, we would see that power increases and efficiency decrease with respect to increasing swirl. Hence, for a given gait, increasing Wi leads to a relative increase in hydrodynamic efficiency (η/η_N), while increasing ζ leads to a decrease in absolute efficiency η. We further remark that comparisons of power and efficiency for swimmers having different gaits (i.e. different values of ξ and ζ) should be undertaken with caution given recent results suggesting that the squirmer model underestimates the true power expenditure of swimming microorganisms (Ito, Omori & Ishikawa 2019).

5. Conclusion

In conclusion, we have studied how flow acting in the azimuthal direction (created by, say, a rotating flagellum) can change swimming kinematics in a viscoelastic fluid. Specifically, we found that when ζ, characterizing the relative extent of the swirling flow, is sufficiently large, that our numerical simulations and asymptotic theory predict a speed enhancement relative to that in a Newtonian fluid. Through an analysis of the polymer stress in the surrounding flow field and the surface tractions acting on the surface of the swimmer, we found that this speed increase is primarily associated with a decrease in the extensional wake behind the swimmer. After systematically varying the swimmer's gait, the fluid rheology, and the constitutive equation used to describe the fluid elasticity, we find that the speed enhancement seen at large values of ζ persists. Furthermore, while the majority of the simulations presented here are conducted at $Re = 0$ and $\alpha_m = 0.2$ (indicating a substantial amount of shear thinning), results conducted at finite Re and for smaller values of α_m actually predict an even greater increase in the swimming speed; hence, our work effectively presents a lower limit on the magnitude of this effect. We concluded our analysis by assessing how the hydrodynamic power and efficiency vary with swirl. For all gaits, increasing fluid elasticity leads to a decrease in power expenditure and an increase in swimming efficiency, with the rate of decrease/increase proportional to the amount of swirl present. Interestingly enough, when comparing across gaits, hydrodynamic power increases strongly in proportion to the amount of swirl present; hence, the gaits with swirl present are less efficient than those without despite the speed enhancement discussed above. By approximating ζ for a true microorganism, we found that a value of $\zeta \approx 4.2$ is typical, indicating that the effect of swirl is likely significant in an elastic fluid. Finally, we believe the phenomenon reported in this manuscript should apply to a wide range of biological organisms since fundamentally it merely requires the coupling of rotational flow to translational velocity via the elasticity of the fluid.

Acknowledgements

J.P.B. is supported by a National Science Foundation (NSF) Graduate Research Fellowship (grant no. DGE – 1656518). A.P. was supported by the Stanford Summer Research Program (SSRP) through the Amgen Foundation. This work is also supported by NSF grant no. CBET 1803765.

Declaration of interests

The authors report no conflict of interest.

REFERENCES

BINAGIA, J. P., GUIDO, C. J. & SHAQFEH, E. S. G. 2019 Three-dimensional simulations of undulatory and amoeboid swimmers in viscoelastic fluids. *Soft Matter* **15** (24), 4836–4855.

BIRD, R. B., ARMSTRONG, R. C. & HASSAGER, O. 1987 *Dynamics of Polymeric Liquids*, Fluid Mechanics, vol. 1. John Wiley and Sons, Inc.

BLAKE, J. R. 1971 A spherical envelope approach to ciliary propulsion. *J. Fluid Mech.* **46** (1), 199–208.

CASTILLO, A., MURCH, W. L., EINARSSON, J., MENA, B., SHAQFEH, E. S. G. & ZENIT, R. 2019 Drag coefficient for a sedimenting and rotating sphere in a viscoelastic fluid. *Phys. Rev. Fluids* **4** (6), 063302.

COSTERTON, J. W., STEWART, P. S. & GREENBERG, E. P. 1999 Bacterial biofilms: a common cause of persistent infections. *Science* **284** (5418), 1318–1322.

DE CORATO, M. & D'AVINO, G. 2017 Dynamics of a microorganism in a sheared viscoelastic liquid. *Soft Matter* **13** (1), 196–211.

DE CORATO, M., GRECO, F. & MAFFETTONE, P. L. 2015 Locomotion of a microorganism in weakly viscoelastic liquids. *Phys. Rev.* E **92** (5), 053008.

DASGUPTA, M., LIU, B., FU, H. C., BERHANU, M., BREUER, K. S., POWERS, T. R. & KUDROLLI, A. 2013 Speed of a swimming sheet in Newtonian and viscoelastic fluids. *Phys. Rev.* E **87** (1), 1–7.

DATT, C. & ELFRING, G. J. 2019 A note on higher-order perturbative corrections to squirming speed in weakly viscoelastic fluids. *J. Non-Newtonian Fluid Mech.* **270** (March), 51–55.

DATT, C. & ELFRING, G. J. 2020 Corrigendum to "A note on higher-order perturbative corrections to squirming speed in weakly viscoelastic fluids" [J. Non-Newtonian Fluid Mech. 270 (2019) 51–55]. *J. Non-Newtonian Fluid Mech.* **277**, 104224.

DATT, C., NATALE, G., HATZIKIRIAKOS, S. G. & ELFRING, G. J. 2017 An active particle in a complex fluid. *J. Fluid Mech.* **823**, 675–688.

DATT, C., ZHU, L., ELFRING, G. J. & PAK, O. S. 2015 Squirming through shear-thinning fluids. *J. Fluid Mech.* **784**.

DRESCHER, K., DUNKEL, J., CISNEROS, L. H., GANGULY, S. & GOLDSTEIN, R. E. 2011 Fluid dynamics and noise in bacterial cell-cell and cell-surface scattering. *Proc. Natl Acad. Sci. USA* **108** (27), 10940–10945.

ELFRING, G. J. & GOYAL, G. 2016 The effect of gait on swimming in viscoelastic fluids. *J. Non-Newtonian Fluid Mech.* **234**, 8–14.

FATTAL, R. & KUPFERMAN, R. 2004 Constitutive laws for the matrix-logarithm of the conformation tensor. *J. Non-Newtonian Fluid Mech.* **123** (2–3), 281–285.

FAUCI, L. J. & DILLON, R. 2006 Biofluidmechanics of reproduction. *Annu. Rev. Fluid Mech.* **38** (1), 371–394.

FELDERHOF, B. U. & JONES, R. B. 2016 Stokesian swimming of a sphere at low Reynolds number by helical surface distortion. *Phys. Fluids* **28** (7), 073601.

FU, H. C., POWERS, T. R. & WOLGEMUTH, C. W. 2007 Theory of swimming filaments in viscoelastic media. *Phys. Rev. Lett.* **99** (25), 258101.

FU, H. C., WOLGEMUTH, C. W. & POWERS, T. R. 2009 Swimming speeds of filaments in nonlinearly viscoelastic fluids. *Phys. Fluids* **21** (3), 033102.

GAO, W. & WANG, J. 2014 Synthetic micro/nanomotors in drug delivery. *Nanoscale* **6**, 10486–10494.

GHOSE, S. & ADHIKARI, R. 2014 Irreducible representations of oscillatory and swirling flows in active soft matter. *Phys. Rev. Lett.* **112** (11), 1–5.

GIESEKUS, H. 1982 A simple constitutive equation for polymer fluids based on the concept of deformation-dependent tensorial mobility. *J. Non-Newtonian Fluid Mech.* **11** (1–2), 69–109.

GODÍNEZ, F. A., KOENS, L., MONTENEGRO-JOHNSON, T. D., ZENIT, R. & LAUGA, E. 2015 Complex fluids affect low-Reynolds number locomotion in a kinematic-dependent manner. *Exp. Fluids* **56** (5), 1–10.

HAM, F., MATTSSON, K. & IACCARINO, G. 2006 Accurate and stable finite volume operators for unstructured flow solvers. In *Center for Turbulence Research Annual Research Briefs*, pp. 243–261. Center for Turbulence Research.

HARMAN, M. W., DUNHAM-EMS, S. M., CAIMANO, M. J., BELPERRON, A. A., BOCKENSTEDT, L. K., FU, H. C., RADOLF, J. D. & WOLGEMUTH, C. W. 2012 The heterogeneous motility of the Lyme disease spirochete in gelatin mimics dissemination through tissue. *Proc. Natl Acad. Sci. USA* **109** (8), 3059–3064.

HOUSIADAS, K. D. 2017 Improved convergence based on linear and non-linear transformations at low and high Weissenberg asymptotic analysis. *J. Non-Newtonian Fluid Mech.* **247**, 1–14.

HOUSIADAS, K. D. 2019 Steady sedimentation of a spherical particle under constant rotation. *Phys. Rev. Fluids* **4** (10), 103301.

HULSEN, M. A., FATTAL, R. & KUPFERMAN, R. 2005 Flow of viscoelastic fluids past a cylinder at high Weissenberg number: stabilized simulations using matrix logarithms. *J. Non-Newtonian Fluid Mech.* **127** (1), 27–39.

ISHIKAWA, T., SIMMONDS, M. P. & PEDLEY, T. J. 2006 Hydrodynamic interaction of two swimming model micro-organisms. *J. Fluid Mech.* **568**, 119–160.

ITO, H., OMORI, T. & ISHIKAWA, T. 2019 Swimming mediated by ciliary beating: comparison with a squirmer model. *J. Fluid Mech.* **874**, 774–796.

KATZ, D. F., MILLS, R. N. & PRITCHETT, T. R. 2008 The movement of human spermatozoa in cervical mucus. *J. Reprod. Fertil.* **53** (2), 259–265.

LAUGA, E. 2007 Propulsion in a viscoelastic fluid. *Phys. Fluids* **19** (8), 083104.

LAUGA, E. 2009 Life at high deborah number. *Europhys. Lett.* **86** (6), 64001.

LAUGA, E. 2016 Bacterial hydrodynamics. *Annu. Rev. Fluid Mech.* **48**, 105–130.

LAUGA, E. & POWERS, T. R. 2009 The hydrodynamics of swimming microorganisms. *Rep. Prog. Phys.* **72** (9), 096601.

LI, G.-J., KARIMI, A. & ARDEKANI, A. M. 2014 Effect of solid boundaries on swimming dynamics of microorganisms in a viscoelastic fluid. *Rheol. Acta* **53** (12), 911–926.

LI, J., DE ÁVILA, B. E.-F., GAO, W., ZHANG, L. & WANG, J. 2017 Micro/nanorobots for biomedicine: delivery, surgery, sensing, and detoxification. *Sci. Robot.* **2** (4), 1–10.

LIGHTHILL, M. J. 1952 On the squirming motion of nearly spherical deformable bodies through liquids at very small reynolds numbers. *Commun. Pure Appl. Maths* **5** (2), 109–118.

LIU, B., POWERS, T. R. & BREUER, K. S. 2011 Force-free swimming of a model helical flagellum in viscoelastic fluids. *Proc. Natl Acad. Sci.* **108** (49), 19516–19520.

MAN, Y. & LAUGA, E. 2015 Phase-separation models for swimming enhancement in complex fluids. *Phys. Rev.* E **92** (2), 1–10.

MARTINEZ, V. A., SCHWARZ-LINEK, J., REUFER, M., WILSON, L. G., MOROZOV, A. N. & POON, W. C. K. 2014 Flagellated bacterial motility in polymer solutions. *Proc. Natl Acad. Sci. USA* **111** (50), 17771–17776.

PADHY, S., SHAQFEH, E. S. G., IACCARINO, G., MORRIS, J. F. & TONMUKAYAKUL, N. 2013 Simulations of a sphere sedimenting in a viscoelastic fluid with cross shear flow. *J. Non-Newtonian Fluid Mech.* **197**, 48–60.

PAK, O. S. & LAUGA, E. 2014 Generalized squirming motion of a sphere. *J. Engng Maths* **88** (1), 1–28.

PAK, O. S., ZHU, L., BRANDT, L. & LAUGA, E. 2012 Micropropulsion and microrheology in complex fluids via symmetry breaking. *Phys. Fluids* **24** (10), 103102.

PATRA, D., SENGUPTA, S., DUAN, W., ZHANG, H., PAVLICK, R. & SEN, A. 2013 Intelligent, self-powered, drug delivery systems. *Nanoscale* **5** (4), 1273–1283.

PATTESON, A. E., GOPINATH, A. & ARRATIA, P. E. 2016 Active colloids in complex fluids. *Curr. Opin. Colloid Interface Sci.* **21**, 86–96.

PATTESON, A. E., GOPINATH, A., GOULIAN, M. & ARRATIA, P. E. 2015 Running and tumbling with *E. coli* in polymeric solutions. *Sci. Rep.* **5**, 15761.

PEDLEY, T. J. 2016 Spherical squirmers: models for swimming micro-organisms. *IMA J. Appl. Maths* **81** (3), 488–521.

PEDLEY, T. J., BRUMLEY, D. R. & GOLDSTEIN, R. E. 2016 Squirmers with swirl: a model for volvox swimming. *J. Fluid Mech.* **798**, 165–186.

PETERLIN, A. 1966 Hydrodynamics of macromolecules in a velocity field with longitudinal gradient. *J. Polym. Sci.* **4** (4), 287–291.

PIETRZYK, K., NGANGUIA, H., DATT, C., ZHU, L., ELFRING, G. J. & PAK, O. S. 2019 Flow around a squirmer in a shear-thinning fluid. *J. Non-Newtonian Fluid Mech.* **268** (April), 101–110.

PUENTE-VELÁZQUEZ, J. A., GODÍNEZ, F. A., LAUGA, E. & ZENIT, R. 2019 Viscoelastic propulsion of a rotating dumbbell. *Microfluid Nanofluid* **23** (9), 108.

PURCELL, E. M. 1977 Life at low Reynolds number. *Am. J. Phys.* **45** (1), 3–11.

RICHTER, D., IACCARINO, G. & SHAQFEH, E. S. G. 2010 Simulations of three-dimensional viscoelastic flows past a circular cylinder at moderate Reynolds numbers. *J. Fluid Mech.* **651**, 415–442.

RILEY, E. E. & LAUGA, E. 2014 Enhanced active swimming in viscoelastic fluids. *Europhys. Lett.* **108** (3), 34003.

ROGOWSKI, L. W., KIM, H., ZHANG, X. & JUNKIM, M. 2018 Microsnowman propagation and robotics inside synthetic mucus. In *2018 15th International Conference on Ubiquitous Robots (UR)*, pp. 5–10. IEEE.

SHEN, X. N. & ARRATIA, P. E. 2011 Undulatory swimming in viscoelastic fluids. *Phys. Rev. Lett.* **106** (20), 208101.

SILLANKORVA, S. M., OLIVEIRA, H. & AZEREDO, J. 2012 Bacteriophages and their role in food safety. *Intl J. Microbiol.* **2012**, 863945.

SPAGNOLIE, S. E. 2015 *Complex Fluids in Biological Systems*, Biological and Medical Physics, Biomedical Engineering. Springer.

SPAGNOLIE, S. E., LIU, B. & POWERS, T. R. 2013 Locomotion of helical bodies in viscoelastic fluids: enhanced swimming at large helical amplitudes. *Phys. Rev. Lett.* **111** (6), 068101.

SUAREZ, S. S. & PACEY, A. A. 2006 Sperm transport in the female reproductive tract. *Hum. Reprod. Update* **12** (1), 23–37.

TERAN, J., FAUCI, L. & SHELLEY, M. 2010 Viscoelastic fluid response can increase the speed and efficiency of a free swimmer. *Phys. Rev. Lett.* **104** (3), 1–4.

THOMASES, B. & GUY, R. D. 2014 Mechanisms of elastic enhancement and hindrance for finite-length undulatory swimmers in viscoelastic fluids. *Phys. Rev. Lett.* **113** (9), 1–5.

THOMASES, B. & GUY, R. D. 2017 The role of body flexibility in stroke enhancements for finite-length undulatory swimmers in viscoelastic fluids. *J. Fluid Mech.* **825**, 109–132.

Wolfram Research, Inc. 2019 Mathematica, Version 12.0. Champaign, IL.

YAN, X., ZHOU, Q., VINCENT, M., DENG, Y., YU, J., XU, J., XU, T., TANG, T., BIAN, L., WANG, Y. X. J., *et al.* 2017 Multifunctional biohybrid magnetite microrobots for imaging-guided therapy. *Sci. Robot.* **2** (12), 1–15.

YANG, M., KRISHNAN, S. & SHAQFEH, E. S. G. G. 2016 Numerical simulations of the rheology of suspensions of rigid spheres at low volume fraction in a viscoelastic fluid under shear. *J. Non-Newtonian Fluid Mech.* **233**, 181–197.

ZHU, L., DO-QUANG, M., LAUGA, E. & BRANDT, L. 2011 Locomotion by tangential deformation in a polymeric fluid. *Phys. Rev.* E **83** (1), 011901.

ZHU, L., LAUGA, E. & BRANDT, L. 2012 Self-propulsion in viscoelastic fluids: pushers vs. pullers. *Phys. Fluids* **24** (5), 051902.

ZÖTTL, A. & YEOMANS, J. M. 2019 Enhanced bacterial swimming speeds in macromolecular polymer solutions. *Nat. Phys.* **15** (6), 554–558.